



City Research Online

## City, University of London Institutional Repository

---

**Citation:** Shaheen, M. A., Tsavdaridis, K. D. & Yamada, S. (2018). Comprehensive FE Study of the Hysteretic Behavior of Steel-Concrete Composite and Noncomposite RWS Beam-to-Column Connections. *Journal of Structural Engineering*, 144(9), 04018150. doi: 10.1061/(asce)st.1943-541x.0002124

This is the accepted version of the paper.

This version of the publication may differ from the final published version.

---

**Permanent repository link:** <https://openaccess.city.ac.uk/id/eprint/27691/>

**Link to published version:** [https://doi.org/10.1061/\(asce\)st.1943-541x.0002124](https://doi.org/10.1061/(asce)st.1943-541x.0002124)

**Copyright:** City Research Online aims to make research outputs of City, University of London available to a wider audience. Copyright and Moral Rights remain with the author(s) and/or copyright holders. URLs from City Research Online may be freely distributed and linked to.

**Reuse:** Copies of full items can be used for personal research or study, educational, or not-for-profit purposes without prior permission or charge. Provided that the authors, title and full bibliographic details are credited, a hyperlink and/or URL is given for the original metadata page and the content is not changed in any way.

---

City Research Online:

<http://openaccess.city.ac.uk/>

[publications@city.ac.uk](mailto:publications@city.ac.uk)

---

# **Comprehensive FE Study of the Hysteretic Behaviour of Steel-Concrete Composite and Non-Composite RWS Beam-to-Column Connections**

**Mohamed A. Shaheen<sup>1\*</sup>, Konstantinos Daniel Tsavdaridis<sup>2</sup>, Satoshi Yamada<sup>3</sup>**

<sup>1</sup>*MSC, Civil Engineering, Al-Azhar University, Cairo, Egypt [mashaheen92@gmail.com](mailto:mashaheen92@gmail.com)*

<sup>2</sup>*Institute for Resilient Infrastructure, School of Civil Engineering, University of Leeds, LS2 9JT, Leeds, UK*

<sup>3</sup>*School of Civil and Environmental Engineering, Tokyo Institute of Technology, Japan*

*\*Corresponding Author*

## **ABSTRACT**

This paper investigates the behaviour of reduced web section (RWS) steel-concrete composite (SCC) beam-to-column connections with circular web openings through a comprehensive finite element (FE) analysis following experimental and computational studies. Results showed that the presence of a circular web opening is effective to move the plastic hinge away from the column shear panel zone and the main connection components, and hence, significantly improve the ductility and energy dissipation of the connection without critically affecting its capacity. The composite action was not considered in the literature to account for the severest case (slab acts as load only) in terms of load carrying capacity. However, this study proves that the composite effect has a decisive role in the calculation of the ductility and rotational capacity, and if not considered may result in an overestimated ductile behaviour. On the other hand, in cases where composite action is not provided depending on the particular flooring system, non-composite steel connections may be considered where the ductility and energy dissipation gains are definitely higher but the load carrying capacity is lower.

This paper establishes the comparison between composite and non-composite connections and concludes that the contribution of the composite action to the load carrying capacity is higher with the increase of the beam web opening diameter. Therefore, the calculated negative load carrying capacity tends to be very conservative if the composite effect is neglected when a large opening diameter is used.

*Keywords:* RWS connections, Plastic hinge, Vierendeel, Ductility, Composite beam-column connection

## 1. Introduction

Due to their good ductility and carrying load capability, steel-concrete composite (SCC) structures are increasingly considered in building design particularly in earthquake-prone regions, while input energy dissipated mainly by the plastic deformation of the structure. Local excessive deformation takes place at high stress concentration regions such as beam-to-column connections. Before the 1994 Northridge earthquake in California and 1995 Kobe earthquake in Japan structural engineers and researchers believed that fully welded connections provide the optimum combination of strength and ductility. However, unexpected brittle fractures at the region of the welded beam-to-column connections were found during these earthquakes (Youssef et al., 1995; Toyoda, 1995). Therefore, the ductility and strength of connections inevitably halt the climax of steel and composite structures when the selected parameters of the connection fail to achieve ductility that tally with the system level. It is worth to note that also prior to these benchmark events, there had been concerns about the performance of the welded beam-to-column connections for severe earthquakes. Studies (Engelhardt and Husain, 1993; Popov et al., 1985) reported that these fully fixed connections demonstrated significant lack of deformation capacity under cyclic loading.

To achieve reliable performance of a structural system, attention should be paid to the location of the plastic hinge such that the system can satisfy the well-known “strong-column weak-beam” mechanism and avoid brittle failure. Particularly, the welded and heated zones of the bottom flange may suffer high inelastic strain demand in case of a plastic hinge formed at the face of the column which may then lead to brittle failure. Similarly, the plastic hinge should not be formed at the panel zone of the column, as this type of failure mechanism will lead to a soft-story mechanism. Thus, the weld and beam flange will suffer large secondary stresses which can also cause brittle failure of the connection. Therefore, the plastic hinge should be formed ideally in the beam, at a predetermined distance away from the face of the column, its

shear panel zone, and its components (i.e., bolts and plates). Different observations were made in previous studies to satisfy the desirable ductility, strength, and brittleness of connections. The method selected to enhance the performance of the connection should remain compatible with the corresponding structural system.

## **2. Connections types achieve strong column-weak beam mechanism**

There are three different methods to achieve strong column-weak beam mechanism. The first method is to strengthen of the connection region (using stiffeners and haunches) to avoid plasticity of any component of the connection and surrounding heated zones (Kim et al., 2004). The second method is to weaken the beam by trimming away steel part(s) from the beam flanges at designated locations (Lee et al., 2005); this method is well known as Reduced Beam Section (RBS). In this method, considerable attention should be paid to the flexural strength and stiffness of the beam so that does not change (decrease) dramatically due to the removed steel parts. Moreover, asymmetrical flange cuts should not affect the lateral (out of plane) stability of the beam with the result to increase the probability of lateral torsional buckling.

More recently, an alternative method has been suggested by cutting-out steel parts from the beam web, the so-called Reduced Web Section (RWS) connections (Tsavdaridis et al., 2014; Tsavdaridis et al., 2016; Yang et al., 2009). The shear strength of the beam at the reduced section is decreased based on the web opening size, and the shear forces transferred across the opening result in secondary moments known as Vierendeel moments. The trimmed steel parts from the beam's web are away from the concrete slab, thus, selecting this retrofitting type is considered as the most effective way in terms of cost and time.

### **3. Scope of the study**

Steel concrete composite beams are used in engineering practice widely since they have considerable higher strength and stiffness compared with the non-composite steel beams. It is worth to note that composite action may increase the non-composite beam's strength by 1.5 times under positive bending moment (Kim et al., 2004; Nakashima et al., 2007). Yet, there have been no studies reported on SCC RWS connections. The existence of slab may be detrimental in some cases since it may cause the section below the opening (bottom tee) to go into compression and the section above the opening (top tee) to go into tension even though the section is subjected to positive bending moment at the opening location (Darwin and Donahey, 1988). Moreover, the seismic resistant design of RWS connections implies they will be subjected to cyclic loading and will reach both positive and negative bending moments which can cause the slab to be reversibly on the tension side. However, limited studies have been conducted considering the behaviour of composite beams with openings in the negative moment (Chen et al. 2011).

Accordingly, the behaviour of RWS connections with composite beams under cyclic loading is worth to be investigated to account for both positive and negative moments. In this paper, RWS connections with composite beams were investigated through comprehensive FE analyses while the FE model was initially validated using an experimental test from the literature (Lee et al., 2016).

### **4. Finite Element Modelling (FEM) and validation**

One of the connections experimentally tested by Lee et al. (2016) was modelled using the general-purpose FE software ABAQUS (2010). The FE models were developed using a three-dimensional continuum with solid elements. The selected specimen was a conventional SCC beam-to-column connection type, often referred as a Pre-Northridge connection (**Fig. 1**).

This type of connection configuration exhibited brittle failure at heated zone during an earthquake, and this was confirmed by the experimental test since brittle failure took place in the bottom flange near the access hole.

### *5.1. Contact surfaces and element type*

The ‘embedded element’ technique from ABAQUS was employed to model the interaction between the slab-reinforcement and the slab-studs. In this technique, the nodes’ translational degrees of freedom of the embedded elements (reinforcement and studs) are constrained to the interpolated values of the corresponding degrees of freedom of the host elements (concrete slab). To simplify the FE model, the interface between the welded parts in the experimental test (such as the column and beam) were modelled as tie constraints. The interface between the slab, the steel beam, and the column were considered as a frictionless formulation and the sliding between the beam and the slab was resisted by the shear stud connection. The normal contact behaviour was defined by using a hard contact in ABAQUS which does not permit transfer of the tensile stress across the interface and constrain the nodes on one surface to penetrate the other surface.

The FE mesh of the elaborated model is shown in **Fig. 2**. Two mesh types were used to achieve appropriate mesh density in the column shear panel zone and the beam parts near the column flange. 8-node linear brick elements with reduced integration (C3D8R) were mainly adopted for the solid parts (i.e., beams, column, slab, plates and, shear studs) considering that fine mesh was assigned for parts expected to receive high stress concentration and coarse mesh for the other parts. For the regions between fine and coarse mesh, a 4-node linear tetrahedron element (C3D4) was adopted as a transition mesh element (**Fig. 2**). The transition mesh was used away from the critical locations. The steel reinforcement was modelled with a truss element type, 2-node linear 3-D truss (T3D2), since such element type can eliminate any resistance to bending, and carries only tensile and compression loads. To simplify the mesh,

the shear stud was modelled by an equivalent rectangular section with the same sectional area of the circular stud used in the test whereas the head of the stud was not modelled. Furthermore, the ribs of the slab were considered rectangular instead of trapezoidal for the ease of modelling. A mesh convergence study was conducted to investigate the effect of mesh size on the accuracy and reliability of the results. The results of the refined model were compared with the original model (coarse elements). The difference in the maximum stress was insignificant (2.6%), therefore, the FE mesh was able to capture accurate results.

## 5.2. Material model

The material nonlinearity of the steel beam ( $f_y = 304$  and  $f_u = 455\text{MPa}$ ) and column ( $f_y = 343$  and  $f_u = 512\text{MPa}$ ) was considered during the analysis by adopting bilinear stress-strain relation. The Von Mises yield criterion with kinematic hardening rule was used to define the plastic behaviour of the beam and the column. The tangent modulus was assumed  $E_t = 1000\text{MPa}$ . An elastic-perfectly-plastic relation was adopted for other steel parts such as steel reinforcement, plates and stiffeners. The Young's Modulus equal to 200GPa and Poisson's ratio equal to 0.3 were assigned for the steel material in the elastic range. In the experimental test, it was reported that the concrete slab adjacent to the column crushed due to the bearing action between the slab and the column flange. In order to account for this behaviour in the FE model, the constitutive model with concrete damage plasticity (CDP) was adopted. The CDP model is capable of representing the concrete crushing and formation of cracks. A constitutive law for the concrete under compression was employed based on EC2 (CEN, 2005) while the tension softening curve was developed using the experimentally verified numerical method as it was proposed by Hilleborg (1989).

### *5.3. Loading and boundary condition*

The load was applied in two subsequent steps. Initially, the self-weight of the structure was considered during the analysis. In the second step, cyclic displacement load was applied at the beam end (i.e., at 3597mm from the column face). The applied displacement was following the AISC cyclic loading protocol (AISC, 2002) as illustrated in **Fig. 3**. In order to resemble the action of the loading apparatus, the applied displacement was distributed on the area represented by the projection area of the contact surface between the actuator and the top flange of the beam. The geometric nonlinearity affects the local stresses due to the second order analysis and may lead to the loss of structural stability. Therefore, the geometric nonlinearity was considered in the analysis through total Lagrange (small strain and large rotation formulation). The analysis was carried out on the imperfect model to account for the geometrical imperfection. In order to introduce a geometric imperfection, Eigen buckling mode shapes were computed in a separate buckling analysis and the first Eigen buckling mode was then employed to perturb the geometry of the ‘perfect’ FE model. The imperfect shape was assumed similar to the first Eigen mode factored by the magnitude of 0.5.

The displacement in the three directions of the hinge support was restricted to the top and the bottom end of the column. In order to avoid restraining the moments and achieve pure hinge behaviour, the end cross section of the column (**Fig. 3**) was tied to a reference point and then the boundary conditions assigned to this reference point. Similar to the experimental test, the out-of-plane direction was restrained for the main beam in the area between the applied displacement and the slab to avoid any out-of-plane deformation outside the tested zone.

### *5.4. Results and comparison with experimental test*

The normalised moment at the column face against the story drift rotation curve obtained from the FE modelling is plotted in **Fig. 4** together with the test data from Lee et al.

(2016) for a direct comparison. The normalised moment was calculated based on the actual plastic moment of the steel beam only. The initial stiffness and post-elastic behaviour compare well between the FE model and the experimental test. However, a mismatch of 8.2% between the two curves was recorded at the maximum capacity when the applied load became downward. It is suggested that the difference occurs due to the simplification used in the FE modelling regarding the boundary conditions and material modelling, and it was considered acceptable. The fracture strain of the bottom flange at the heated zones was compared against the value captured in the experimental test. The rupture strain captured from the FE model was slightly lower than the corresponding value in the test (approximately ~3%). The equivalent plastic strain (PEEQ) obtained at the rotation corresponding to the rupture of the bottom flange due to the experimental test is shown in **Fig. 5**. It is depicted that the strain concentrated near the column flange and around the access hole causes the initiation of crack in the weld and led to the sudden failure of the connection. Also, the damage of the concrete was similar for both the experimental test and the FE model, as it is demonstrated in **Fig. 6**. Overall, it was concluded that the FE model was appropriate to be employed to conduct the parametric analysis of the composite RWS connections under cyclic loading.

## 5. Geometric parameters

Perforated beams with different geometric parameters were considered in this study. Both composite and non-composite connections (i.e., without considering the concrete slab) with the same web opening parameters were analysed simultaneously for every case to identify the composite action effects on the behaviour and load carrying capacity of the RWS connections. The effect of the opening depth  $d_0$  and the distance between the face of the column to the centreline of the web opening  $S$  (**Fig. 7**) are investigated. Three different values for  $d_0$  and five values for  $S$  parameters were considered as follows:

- $d_0 = 0.5h, 0.67h, \text{ and } 0.75h$
- $S = 0.5h, 0.75h, h, 1.25h, \text{ and } 1.5h$ , where  $h$  is the overall section height of the steel beam.

The slab deck profile, its material, and its thickness were kept the same for all models, similar to what was used in the validated model. Stresses, cracks, and damages developed in the slab required further investigation to accurately refine the mesh and the process is computationally time expensive. Therefore, some models were selected based on their performance and re-analysed following mesh refinement of the slab to carefully study cracks and crushing during the loading processes.

As it was also noted by Baskar et al. (2002), the connection of the node between the steel beam and the concrete slab or between the concrete slab and the steel decking can cause numerical instability and termination of analysis; thus, the metal decking was not considered during the analysis. The presence of metal decking does not affect the strength of the connection as the maximum capacity is governed primarily by the degree of composite action (i.e., the number of shear studs). However, it should be noted that the presence of the metal decking affects the crack pattern in the concrete slab (Darwin 2000).

Specimens were identified by a specific three field identifier as illustrated in **Fig. 8**. The first identifier represents the type of the connection (composite or non-composite), the second identifier represents the diameter of the opening as a percentage of the beam depth ( $h$ ), and the third identifier indicates the end distance as a percentage of the beam depth ( $h$ ).

## **6. Results of parametric study**

### *7.1. Failure criteria of the FE model*

The weld fracture limit state may control the capacity of the connection considering that the weld fails at lower load levels before other failure mechanisms occur such as the local

buckling or the Vierendeel mechanism. Researchers have concluded that equivalent plastic strain (PEEQ) is an indicator for the fracture mechanism for the flanges at welded (heated) zones (Perez, 2004; Chi et al., 2006). Eventually, the failure of the connection was identified by one of the following three situations: (i) local instability due to buckling of the web or the flange, (ii) Vierendeel mechanism, and (iii) rupture of the bottom flange at the heated zone. The local instability and the Vierendeel mechanism can be captured accurately by considering the geometric nonlinearity of the imperfect model in ABAQUS. The heated zone is susceptible to brittle failure due to the stress concentration at the weld. Therefore, the rupture of the bottom flange near the column face found by monitoring the PEEQ during the analysis. The fracture strain was identified from the validated model and it was compared against the experimental test (**Fig. 5**). When the strain concentrated away from the column face (far from the heated zone), the failure of the connection characterised by the local buckling or the Vierendeel mechanism (even if the strain exceeded the predefined fracture strain), as it was observed in the experimental tests (Lee et al., 2016; Yang et al., 2009). When the local buckling or the Vierendeel mechanism takes place, it was considered that the failure of the connection was reached when the strength of the connection degraded by 20% from the maximum recorded capacity.

## *7.2. Ductility and failure mode*

It is common in engineering practice the connection strength to be calculated based on the non-composite connection (Eurocode 4, 2005) (i.e., the effect of the slab is neglected). Therefore, the behaviour of the non-composite connection was benchmarked as the reference point in the current study. The ductility and the failure mode of the connection can be revealed by studying the hysteretic curves, in specific the ultimate rotation and strength degradation. The hysteretic curves were developed based on the normalised moment (the applied

moment/plastic moment of steel section) of the beam at the column face and the rotation at the centre line of the column. The summary of the FEA results for the composite RWS connections is given in **Table 1**. The summary of the failure modes captured during the study is summarised in **Fig. 9** to **Fig. 11**.

The PEEQ exceeded the limit value for the flanges of composite and non-composite connection without the web opening (solid-webbed beam), which indicates rupture of the flange as the main failure mode. The composite action resulted in the upward shift of the neutral axis which led to the concentration of the strain on the bottom flange as it is shown in specimen P-NA-NA in **Fig. 9**. Oppositely, the strain in the flanges was well distributed in the unperforated non-composite connections which caused the failure to occur at a higher rotation (**Fig. 12**) and exhibited better performance in terms of ductility.

The failure modes of the RWS connections with composite beams were more complex due to the weak local shear stiffness at the web opening location. Consequently, the secondary moment resulted from the transfer of shear forces along the opening length (Vierendeel moments). Furthermore, Vierendeel mechanism caused different failure modes to be observed for the RWS connections depending on the geometric parameters of the web opening (i.e.,  $d_0$  and  $S$ ).

When small diameter web openings were used (e.g.,  $0.5h$ ), the capacity of the remaining part of the steel section was capable enough to resist the Vierendeel moment. Hence, the Vierendeel mechanism was not captured in the vicinity of the web openings with a small diameter and the failure was mainly due to the local buckling (in case of small  $S$ ) as it is illustrated in **Fig. 10**, or the rupture of the bottom flange (in case of large  $S$ ). When a web opening with small diameter and large end distance,  $S$  (e.g., specimen P-50d-125S) used, the design was not adequate to mobilise the stresses away from the column face and the failure mode was the rupture of the beam's bottom flange as demonstrated in **Fig. 9**, similar to the

unperforated composite connection. Although the capacity of the RWS connections with large end distances is higher than the non-composite connection with a solid-webbed beam, the premature failure has a serious adverse consequence on the ductility (see **Table 1**). For instance, the maximum positive rotation capacities recorded by the connections P-50d-125S and P-50d-150S were 0.03 rad comparing with 0.04 rad for the non-composite unperforated connection which implies that the ductility reduced by roughly 30%. The Vierendeel bending forces increase with the increase in the critical opening length,  $c$  (Darwin, 1988; Chung et al., 2001; Tsavdaridis and D’Mello, 2012a and 2012b). Therefore, the connections with large opening diameters (e.g.,  $d_0$  equal to  $0.67h$  or  $0.75h$ ) suffered high Vierendeel moments which exceeded the Vierendeel capacity of the tee sections. Accordingly, the predominant failure of the connection with large web openings was the Vierendeel mechanism, independent of the end distance (**Fig. 11**).

The ductility of the connection was significantly increased when the web opening introduced is having certain geometric parameters. The composite effect was responsible for the deterioration of the unperforated composite section due to stress concentration and premature rupture of the flanges. The ductility was decreased from 4.21 to 3.09 (26.6%) when the slab added to the unperforated non-composite connection (**Table 1**). However, the use of the web opening, such as in model P-50d-50S, enhanced the ductility in the positive and the negative directions by 32% and 70%, respectively. This enhancement has a great positive effect on the dissipated energy which was increased by 130% without affecting the negative ultimate strength significantly.

In addition, it was concluded that the ductility depends highly on the failure mode of the connection. In the case of local buckling, the strength degradation was insignificant compared to one when rupture of the flange or Vierendeel mechanism is recorded. Consequently, a higher number of cycles were needed before the strength was reduced to the

80% of the maximum recorded strength; the point at which the failure is assumed. **Fig. 13** depicts the hysteretic curves of two specimens with different failure modes plotted against the reference non-composite connection. The negative capacity of the connection P-75d-75S was recorded in cycle number three (at 0.014 rad) followed by a slight strength degradation up to 0.02 rad. The Vierendeel mechanism was observed, hence, the strength degradation was relatively high in the next cycle which led to failure. Despite the capacity of the connection P-50d-50S was recorded in the same cycle (at 0.019 rad), the ductility and energy dissipation were significantly higher than the other RWS connections. This was attributed to the strength which was slightly decreased due to the local buckling failure. Therefore, it is suggested to avoid the Vierendeel mechanism as well as the rupture of the flange in order to achieve high ductility using composite RWS connections.

Furthermore, the strength degradation may be responsible for what previous studies reported as high ductility in non-composite RWS connections (Tsavdaridis and Papadopoulos, 2016; Hedayat and Celikag, 2009). The same connection similar to P-50d-50S was analysed without the concrete slab (connection R-50d-50S). It was observed that the strength degradation in the non-composite connection was similar in comparison with the composite connection, as it is shown in **Fig. 14**. The strength of the non-composite connection was decreased slightly by approximately 4% in the last cycle. The strength of the composite connection reduced by more than 15% and 48% when the failure mode was the local buckling or the Vierendeel mechanism, respectively. The number of load cycles before the failure took place was higher in the case of the non-composite connections. Accordingly, the area under the hysteretic curve (defining the energy dissipated) was significantly increased compared with the composite connections. The energy dissipated by the connection R-50d-50S was 30% higher than the connection P-50d-50S, thus, it is concluded that although in previous studies the composite effect was neglected in order to represent the worst case scenario in terms of ultimate

capacity, the composite effect should be considered for RWS connections since its effect may be detrimental on the ductility and the rotational capacity.

### *7.3. Damage of the slab*

From **Fig. 15** it can be concluded that the location and the degree of concrete damages were highly affected by the presence of the web opening. The figure compares the cracking and the crushing of the concrete in unperforated and RWS connections. The connection with the perforated beam suffered a high degree of damages due to the stress concentration in the vicinity of the opening. Cracks were developed in the conventional composite connection at the location of the high bending moment (near the column face). The first crack was observed at 0.008 story drift and then propagated across the entire width of the slab at 0.012 story drift. For RWS connections, the first crack was initiated at the location of the web opening at 0.005 story drift and extended across the entire width of the concrete slab at 0.0085 story drift. The concrete crushing observed near the column face in the unperforated connection was resulted from the bearing between the concrete and the column flange as it is shown in **Fig. 15b**. In RWS connections, concrete crushing was concentrated around the web opening zone as a result of the stress concentration in the slab due to the Vierendeel action.

Severe cracks found in the slab around the opening zone and suggest that the steel reinforcement ratio is important to control the crack width to improve the behaviour of the composite RWS connection. In addition, the concrete strength may play an important role to avoid the crushing of the concrete at an early stage of the loading.

The tension crack and concrete crush of two FE models with different web opening diameters were extracted and plotted in **Fig. 16** to demonstrate the effect of the web opening area (WOA) on the damage of the concrete slab. The concrete damage was compared at the same rotation angles, -0.02 rad for tension crack and 0.02 rad for concrete crushing. **Fig. 17**

compares between the hysteretic responses of the two connections (P-67d-150S and P-75d-150S). The negative capacity at -0.02 rad of the connection with opening diameter  $0.75h$  was lower by roughly 10%. However, the tension cracks observed in this specimen are significantly higher than the specimen with the higher moment. This may attribute to the Vierendeel deformation of the specimen with large WOA which was considerably high as it is illustrated in **Fig. 18**. The observation of the concrete damage under positive direction reveals that the concrete crushing at the opening location was severe when the WOA was increased due to the increase in the applied Vierendeel moments. In conclusion, it becomes apparent that a slight increase in the opening diameter (e.g., by 12%) had a considerable negative effect on the damage and cracks developed in the concrete slab.

#### *7.4. Composite effect*

The capacity of the composite RWS and non-composite connections in both directions was obtained from the FE models and summarized in **Table 1** and **Table 2** to study the contribution of the slab.

It was observed that the positive and negative capacities of the composite RWS connections were higher than the capacities of the non-composite connections (see composite contribution column in **Table 2**, all values are larger than unity. However, the composite effect was significantly influential in the positive direction (when the slab was under compression). The composite effect in the positive direction was approximately 20% higher than the effect in the negative direction. Moreover, the composite effect vary for RWS connections with different opening sizes. While the average contribution of the composite connection in the positive direction was 25.9% for small WOA, that changed to 65.5% when openings with large WOA were used.

The negative bending moment of the composite connection without web opening increased only by 2.7% in comparison with the non-composite unperforated connection.

Therefore, calculating the capacity of the unperforated composite connection under negative moment without including the composite effect is adequate. Similarly, the capacity of the composite RWS connection can be estimated accurately under negative moment without including the composite effect when a small opening is used since the average effect of composite found to be only 3.2%. However, the average effect of the composite action when a large web opening introduced was found to be significant. For instance, the increase in negative capacity of the composite RWS connection was 31.4% in relation to the non-composite connection, when the opening depth was  $0.75h$ . Therefore, the calculated negative capacity tends to be very conservative in case the composite effect is neglected when large WOA is used. The composite effect was independent of the end distances. **Table 2** confirms that the capacity of the composite RWS connection with the same opening depth is approximately similar when different end distances are used.

The increase in strength due to composite action is commonly neglected in engineering practice since the capacity is calculated based on the non-composite connection. Therefore, the actual strength of the beam becomes much higher than the column's strength which causes the plastic hinge to be located in the column or in the weld zone. The increase in strength should be considered during the calculation of beam/column strength ratio to achieve the strong column-weak beam requirement.

In particular, the contribution of the slab to the Vierendeel action, and the strain in the concrete at the opening location were studied. The strain found in the slab of the RWS connection was compared with the strain found in the solid-webbed beam at three different locations with respect to the opening namely: low moment side (LMS), at centreline (CL), and high moment side (HMS). Strain evaluations extracted from model PA-50d-75S were plotted against the strains recorded from the conventional composite connection P-NA-NA as it is depicted in **Fig. 19**. The recorded strains for the RWS connection at LMS and CL of the

opening were higher than the strains at same locations in the unperforated composite connection by only 5%. However, at HMS, the strains in the RWS were significantly higher than the unperforated connection (46%). Therefore, the slab contributes significantly to the strength of the connection. This result, also confirms that the concrete crushing in the vicinity of the opening happened due to the Vierendeel action.

### *7.5. Stress and strain distribution*

The location of the plastic hinge and the behaviour of the connection were studied by investigating the stress and equivalent plastic strain (PEEQ) distribution along the beam. The shear stress in the steel beam is mainly resisted by the web while the bending stress is resisted by the flanges. When low shear forces are considered in comparison with the bending stresses, the bending and shear stresses can be studied separately since the interaction between them is little and can be neglected. By introducing the web opening, the shear resistance was reduced significantly, and therefore, the interaction between the stresses should be considered. The Von Mises stress is suitable to predict the yielding under such combined loading, hence they were extracted at the maximum negative rotation experienced by the connection (**Fig. 20**) to investigate the effect of opening parameters on stress concentration and location of the plastic hinge. The PEEQ was recorded at the failure load in order to predict the location of strain concentration and potentially the steel rupture (**Fig. 21**).

#### *7.5.1. Effect of end distance*

It is generally observed that the opening diameter required to mobilise the stress away from the welded area primarily depend on its location with respect to the column face. The stress zones along the beam can be, conceptually, divided into three parts namely: high stress zone (near to the column face), low stress zone (away from the column face), and medium

stress zone (in between). When the short end distance is used ( $0.5h$ ), a smaller effective WOA is required to attract stress concentration away from the welded area and gain in ductility and energy dissipation without damaging the connection components. Oppositely, a larger end distance ( $1.5h$ ) could be adopted when a large web opening is used to weaken the beam at that location.

When composite connections were examined, more stresses are found concentrated in the panel zone, hence the effect of the web opening was lower. However, when small web opening with short end distance (see specimen P-50d-50S in **Fig. 20**) was used, the opening managed to attract more stresses in case of composite beam.

#### 7.5.2. *Effect of WOA*

For both composite and non-composite connections, the web opening diameter ( $d_0$ ) has significant influence on the stress distribution at the opening location. The stress was concentrated in the beam's flanges when small opening diameter was used. Despite the specimen P-50d-50S experienced stress concentration in the top flange at the weld area, the PEEQ in the top flange at this location was very low which implied that the rupture of the flange will not occur. On the other hand, the Vierendeel behaviour was clearly observed when the large web opening diameter was used while the stress mainly concentrated in the vicinity of the web opening at a specific angle from the centre of the opening (see specimens R-75d-150S and P75d-150S).

This strain concentration may lead to the web tearing at the opening location as observed by Yang et al. (2009). In that experimental test, one of the connections failed by the web tearing, however, the failure of the connection was ductile. For non-composite RWS connections, a high concentration of PEEQ was captured in the vicinity of the opening web as it is illustrated in **Fig. 21**. Adversely, due to the contribution of the slab, the PEEQ was low in

the composite connections. Therefore, the non-composite connections are more susceptible to the web tearing failure.

Overall, the stress and PEEQ were concentrated mainly in the welding zone and the column panel zone for the unperforated composite and non-composite connections. Ultimately, the rupture of the flange occurred when the PEEQ exceeded the limiting value. In the case of the non-composite connections with perforated beams, the yielding was promoted in the vicinity of the web opening and there was no stress or strain concentration observed at the weld location. This observation reveals that the web opening is generally effective to mobilize the stress away from the critical zones. Besides, it is concluded that the design with having web opening with small diameter and short end distance is more effective in reducing the stress around the connection and leads to more ductile behaviour.

## **7. Concluding remarks**

A comprehensive computational study was carried out to investigate the behaviour of the RWS steel-concrete composite beam-to-column connections with isolated circular web openings and compare with the corresponding designs of non-composite connections. The FE model used in the parametric analysis was initially validated against an experimental test found in the literature. This paper focuses on the effect of the opening diameter  $d_0$  and the distance between the face of the column to the centreline of the web opening  $S$ . Based on the analysis, the following conclusions can be drawn:

- The composite effect should be considered during the investigation of RWS connections since it has a detrimental effect on the ductility and the rotational capacity.
- The design of isolated circular web openings with certain parameters ( $d_0$  and  $S$ ) can significantly control and improve the performance of the composite connection,

while the position of the plastic hinge can be effectively mobilised away from the column flange to the location of the opening. For instance, in specimen P-50d-50S, the ductility was increased by 29% and 50% in the positive and the negative directions, respectively. This enhancement has a prodigious positive effect on the dissipated energy which was increased by 135% without affecting the load carrying capacity of the connection.

- Concrete crushing taken place near the column face in the conventional beam-to-column composite connection results from the bearing between the concrete and the column flange. In the case of RWS composite connections, crushing and tension cracks of the slab are concentrated around the web opening. Furthermore, the level of the damage increases with the increase in the diameter of the opening.
- Under negative bending moment, the contribution of the composite action to load carrying capacity tends to be higher in the connections using openings with large diameters (e.g.,  $0.75h$ ). For example, a reasonable composite action increase by only 3.2% in the negative capacity was achieved when the diameter of the opening was  $0.5d_0$  of the section depth; however, this value was increased to be 31.4% when the diameter of the opening was  $0.75d_0$ . Consequently, the calculated negative capacity tends to be very conservative when the composite effect is neglected when large opening diameter is used.

This paper synthesizes all the observations needed to allow engineers to have a reasonable justification as to what should be the balance between the size and location of the circular web opening when composite RWS beam-to-column connections are considered and calculate the moment capacity, the rotational capacity, and the energy dissipation. Similarly,

the results of this paper can be adopted to adjust the performance characteristics of non-composite RWS beam-to-column connections.

## **8. Acknowledgements**

The first author would like to express his gratitude to Japan International Cooperation Agency (JICA) for their financial support to follow the Earthquake Engineering Disaster Mitigation course. The second author would like to acknowledge the contribution of the EPSRC DTG CASE support (EP/L504993/1) and the Institution of Structural Engineers (IStructE) for their continuous technical and financial support.

## **References**

- ABAQUS Version 6.10, 2010. User Documentation, Dassault Systems.
- AISC, American Institute of Steel Construction, 2002. Seismic provisions for structural steel buildings, American Institute of Steel Construction.
- Baskar, K., Shanmugam, N.E. and Thevendran, V., 2002. Finite-element analysis of steel–concrete composite plate girder. *Journal of Structural Engineering*, 128(9), pp.1158-1168.
- CEN (Eurocode 2), 2005. Design of concrete structures – Part 1 – 1: general rules and rules for buildings Brussels: European Standards.
- Chen, T., Gu, X. and Li, H., 2011. Behavior of steel-concrete composite cantilever beams with web openings under negative moment. *International Journal of Steel Structures*, 11(1), pp.39-49.
- Chi, W.M., Kanvinde, A.M. and Deierlein, G.G., 2006. Prediction of ductile fracture in steel connections using SMCS criterion. *Journal of structural engineering*, 132(2), 171-181.

Darwin, D., 1988. Behavior and design of composite beams with web openings. *Steel-Concrete Composite Structures: Stability and Strength*, 55.

Darwin, D. and Donahey, R.C., 1988. LRFD for composite beams with unreinforced web openings. *Journal of Structural Engineering*, 114(3), pp.535-552.

Darwin, D., 1990. Steel and composite beams with web openings: design of steel and composite beams with web openings (Vol. 2). American Institute of Steel Construction.

Darwin, D., 2000. Design of composite beams with web openings. University of Kansas Center for Research, Inc.

Engelhardt, M.D. and Husain, A.S., 1993. Cyclic-loading performance of welded flange-bolted web connections. *Journal of Structural Engineering*, 119(12), 3537-3550.

Eurocode 4, 2005. Design of composite steel and concrete structures – Part 1 – 1: general rules and rules for buildings. British Standards Institution.

Hedayat, A.A. and Celikag, M., 2009. Post-Northridge connection with modified beam end configuration to enhance strength and ductility. *Journal of Constructional Steel Research*, 65(7), 1413-1430.

Hillerborg, A., 1989. Stability problems in fracture mechanics testing in fracture of concrete and rock. In *International Conference on Recent Developments in the Fracture of Concrete and Rock*, 369-378.

Kim, Y.J., Oh, S.H. and Moon, T.S., 2004. Seismic behavior and retrofit of steel moment connections considering slab effects. *Engineering structures*, 26(13), 1993-2005.

Lee, C.H., Jeon, S.W., Kim, J.H. and Uang, C.M., 2005. Effects of panel zone strength and beam web connection method on seismic performance of reduced beam section steel moment connections. *Journal of Structural Engineering*, 131(12), 1854-1865.

Lee, C.H., Jung, J.H., Kim, S.Y. and Kim, J.J., 2016. Investigation of Composite Slab Effect on Seismic Performance of Steel Moment Connections. *Journal of Constructional Steel Research* 117 (2016): 91-100.

Perez N., "fracture mechanics", New York: Kluwer Academic Publishers (2004)

Popov, E.P., Amin, N.R., Louie, J.J. and Stephen, R.M., 1985. Cyclic behavior of large beam-column assemblies. *Earthquake Spectra*, 1(2), 203-238.

Toyoda, M., 1995. How steel structures fared in Japan's great earthquake. *Welding Journal*, 74(12), 31-42.

Tsavdaridis, K.D., Faghih, F. and Nikitas, N., 2014. Assessment of perforated steel beam-to-column connections subjected to cyclic loading. *Journal of Earthquake Engineering*, 18(8), 1302-1325.

Tsavdaridis, K.D. and Papadopoulos, T., 2016. A FE parametric study of RWS beam-to-column bolted connections with cellular beams. *Journal of Constructional Steel Research*, 116, 92-113.

Tsavdaridis, K.D. and D'Mello, C. (2012a) Vierendeel Bending Study of Perforated Steel Beams with Various Novel Shapes of Web Openings, through Non-Linear Finite Element Analyses. *ASCE Journal of Structural Engineering*. 138(10), 1214-1230.

Tsavdaridis, K.D. and D'Mello, C. (2012b) Optimisation of Novel Elliptically-Based Web Opening Shapes of Perforated Steel Beams. *Journal of Constructional Steel Research*. 76, 39-53.

Youssef, N.F., Bonowitz, D. and Gross, J.L., 1995. A survey of steel moment-resisting frame buildings affected by the 1994 Northridge earthquake. US National Institute of Standards and Technology.

Yang, Q., Li, B. and Yang, N., 2009. Aseismic behaviors of steel moment resisting frames with opening in beam web. *Journal of Constructional Steel Research*, 65(6), 1323-1336.

**Table 1:** FE results of the composite connections

Connection notation	Slab	Opening parameters		Max moment		Initial Stiffness (kN.m/rad)		Yield rotation $\theta_y$ (rad)		Ultimate rotation $\theta_u$ (rad)		Ductility $D=\theta_u/\theta_y$		Dissipated energy E (kN.m)	Failure mode
		$d_0$ (mm)	$S$ (mm)	$\frac{M_P^{+ve}}{M_{pl}}$	$\frac{M_P^{-ve}}{M_{pl}}$	$K^{+ve}$	$K^{-ve}$	$\theta_y^{+ve}$	$\theta_y^{-ve}$	$\theta_u^{+ve}$	$\theta_u^{-ve}$	$D^{+ve}$	$D^{-ve}$		
R-NA-NA	NA	NA	NA	1.048	1.023	148378	164618	0.0095	0.0089	0.04	0.03	4.21	3.37	254.78	RTF
P-NA-NA	Yes	NA	NA	1.291	1.051	216687	172492	0.0097	0.0087	0.03	0.03	3.09	3.45	106.11	RBF
P-50d-50S	Yes	350	350	1.223	0.934	213585	170264	0.0090	0.0070	0.05	0.04	5.56	5.71	588.10	LB
P-50d-75S	Yes	350	525	1.234	1.001	214532	170080	0.0095	0.0086	0.04	0.036	4.21	4.19	396.10	LB
P-50d-125S	Yes	350	875	1.254	1.080	215192	175767	0.0100	0.0095	0.03	0.03	3.00	3.16	274.00	RBF
P-50d-150S	Yes	350	1050	1.291	1.051	216687	172492	0.0107	0.0098	0.03	0.03	2.80	3.06	206.09	RBF
P-67d-50S	Yes	469	350	1.097	0.847	203477	164420	0.0095	0.0070	0.04	0.03	4.21	4.29	344.52	VM
P-67d-75S	Yes	469	525	1.150	0.898	208750	164865	0.0097	0.0078	0.04	0.03	4.12	3.85	332.31	VM
P-67d-125S	Yes	469	875	1.242	0.996	210494	167612	0.0098	0.0083	0.04	0.03	4.08	3.61	348.35	VM
P-67d-150S	Yes	469	1050	1.266	1.032	210677	164827	0.0102	0.0085	0.04	0.03	3.92	3.53	361.16	VM
P-75d-50S	Yes	525	350	1.062	0.794	199416	152681	0.0080	0.0063	0.04	0.03	5.00	4.76	297.23	VM
P-75d-75S	Yes	525	525	1.065	0.832	204251	158577	0.0092	0.0065	0.03	0.027	3.26	4.15	186.19	VM
P-75d-125S	Yes	525	875	1.165	0.915	206680	161968	0.0097	0.0076	0.03	0.025	3.09	3.29	185.35	VM
P-75d-150S	Yes	525	1050	1.192	0.932	206835	167785	0.0102	0.0080	0.03	0.021	2.94	2.63	177.00	VM

$M_{pl}$  (plastic moment) = 1927.72kN.m

$M_P^{+ve}$ : Maximum capacity in positive direction for the composite RWS connections

$M_P^{-ve}$ : Maximum capacity in negative direction for the composite RWS connections

RTF: Rupture of the Top Flange

RBF: Rupture of the Bottom Flange

LB: Local Buckling

VM: Vierendeel Mechanism

**Table 2:** FE results of non-composite RWS connections and contribution of composite action

Connection notation	Concrete slab	$d_0$ mm	$S$ mm	Maximum moment		Composite contribution		Average contribution	
				$\frac{M_R^{+ve}}{M_{pl}}$	$\frac{M_R^{-ve}}{M_{pl}}$	$\frac{M_P^{+ve}}{M_R^{+ve}}$	$\frac{M_P^{-ve}}{M_R^{-ve}}$	+ve	-ve
R-50d-50S	NA	350	350	0.940	0.916	1.301	1.019		
R-50d-75S	NA	350	525	0.974	0.952	1.267	1.052	1.259	1.032
R-50d-125S	NA	350	875	1.030	1.036	1.217	1.042		
R-50d-150S	NA	350	1050	1.031	1.037	1.252	1.014		
R-67d-50S	NA	469	350	0.781	0.764	1.405	1.108		
R-67d-75S	NA	469	525	0.804	0.782	1.430	1.148	1.432	1.162
R-67d-125S	NA	469	875	0.855	0.834	1.452	1.194		
R-67d-150S	NA	469	1050	0.880	0.861	1.439	1.199		
R-75d-50S	NA	525	350	0.648	0.631	1.638	1.258		
R-75d-75S	NA	525	525	0.659	0.642	1.615	1.296	1.655	1.314
R-75d-125S	NA	525	875	0.693	0.676	1.683	1.353		
R-75d-150S	NA	525	1050	0.707	0.691	1.686	1.348		

$M_{pl}$  (plastic moment) = 1927.72kN.m

$M_R^{+ve}$ : Maximum capacity in positive direction for the non-composite RWS connections

$M_R^{-ve}$ : Maximum capacity in negative direction for the non-composite RWS connections

$M_P^{+ve}$ : Maximum capacity in positive direction for the composite RWS connections, see **Table 1**

$M_P^{-ve}$ : Maximum capacity in negative direction for the composite RWS connections, see **Table 1**

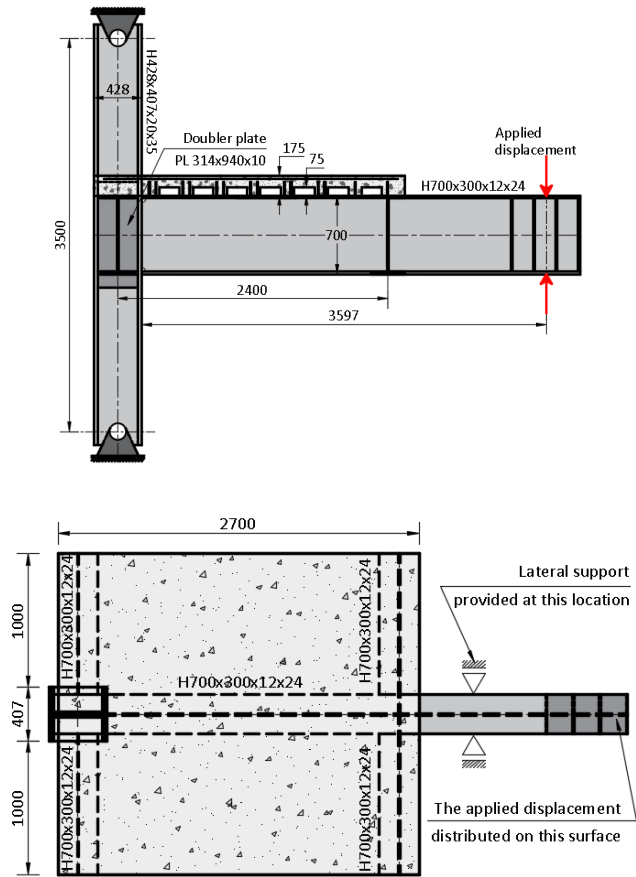


**Fig. 1:** Geometry of the model

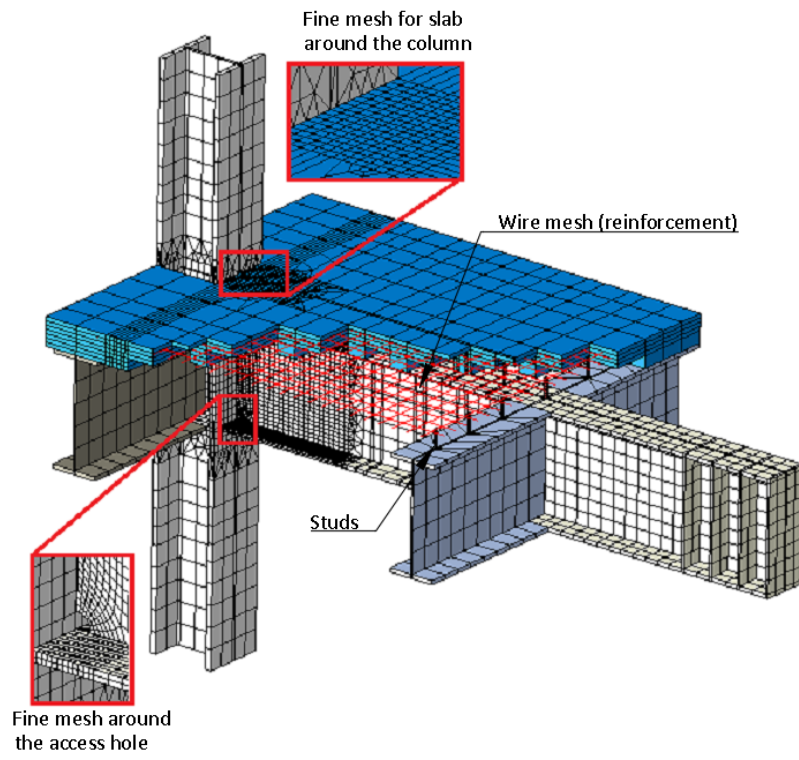


**Fig. 2:** Finite element mesh

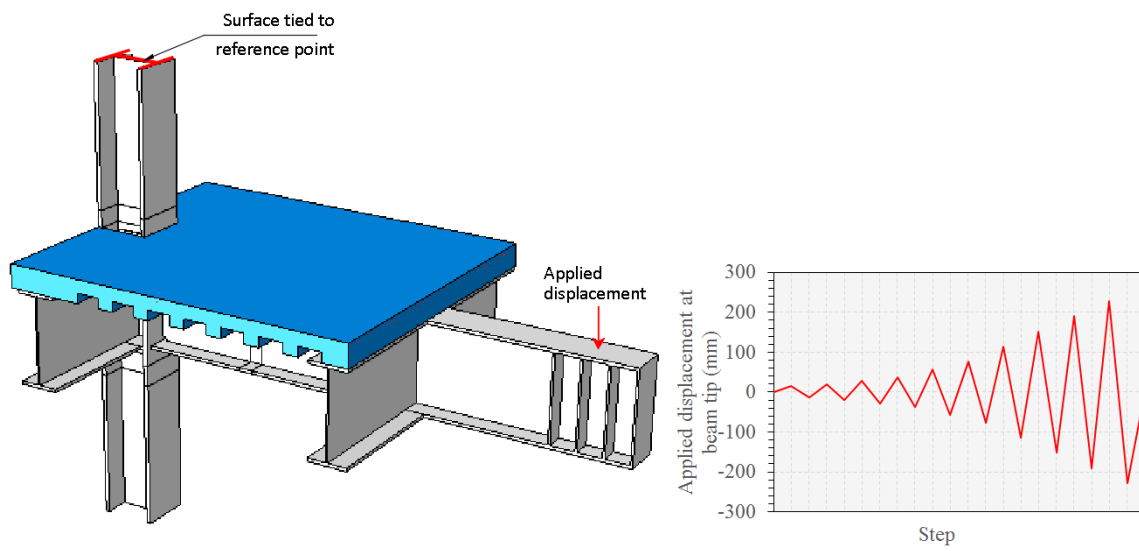


**Fig. 3:** Loading and Boundary conditions

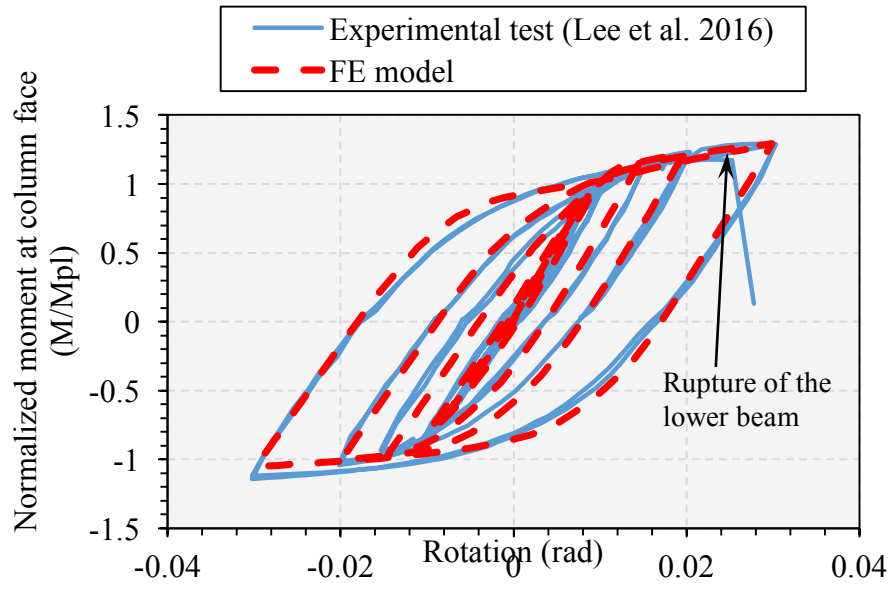


**Fig. 4:** Comparison between analytical and experimental results

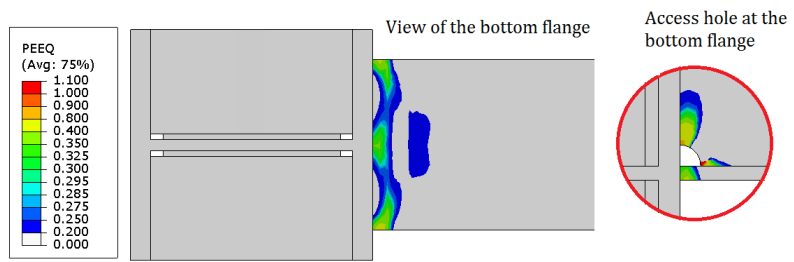


**Fig. 5:** PEEQ at failure rotation



**Fig. 6:** Comparison between crushing of concrete slab (3% rotation)

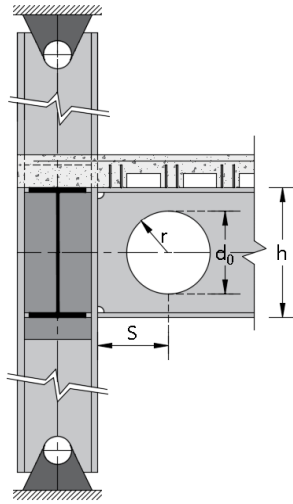


**Fig. 7:** Geometric parameters  $d_0$  and  $S$  with opening configuration

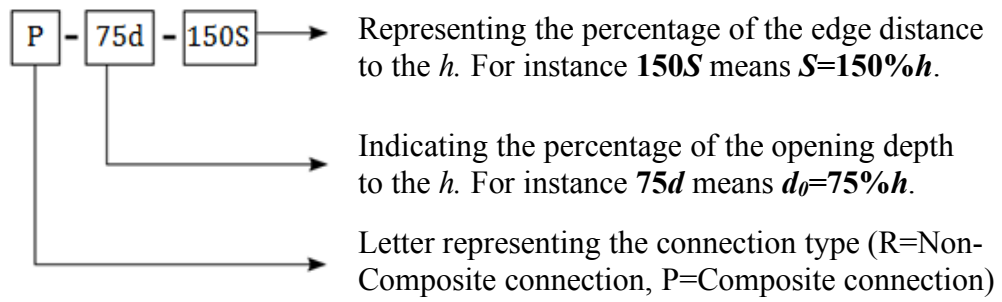


**Fig. 8:** Specimen identifier

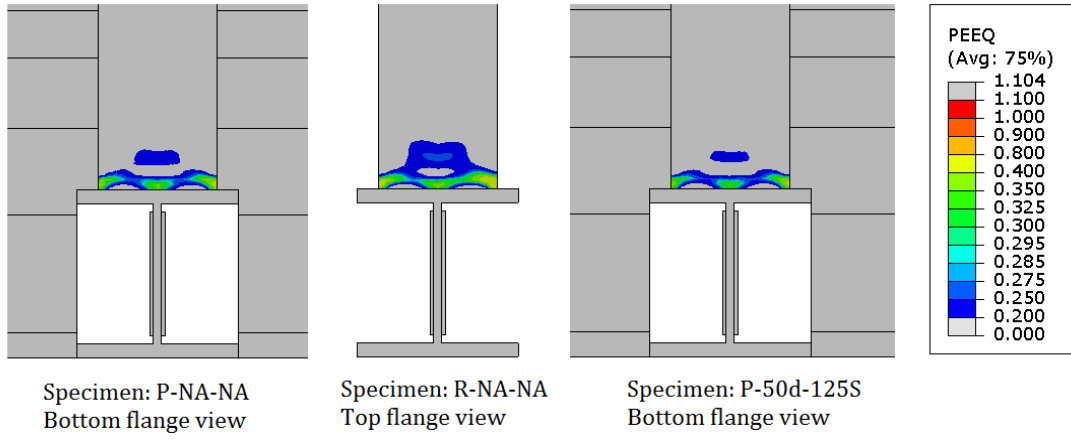
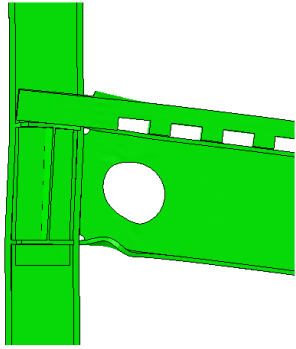
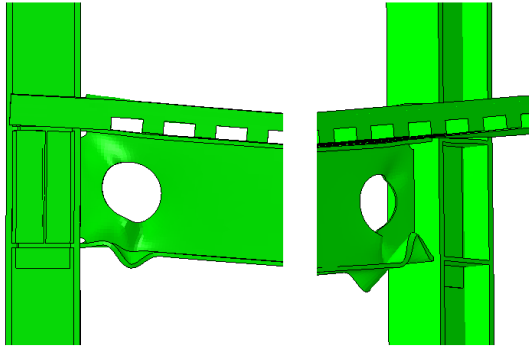


**Fig. 9:** Rupture of the flange (plot PEEQ)

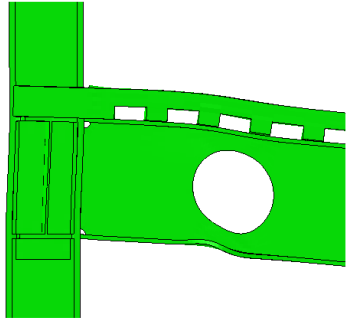


Specimen: P-50d-50S  
Flange buckling (at -2% rotation)

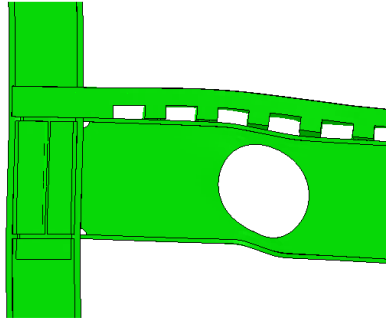


Specimen: P-50d-50S  
Web buckling after  
flange buckling (at -4% rotation)

**Fig. 10:** Local buckling



Specimen: P-67d-125S  
Vierendeel mechanism  
(at -2% rotation)



Specimen: P-75d-150S  
Vierendeel mechanism  
(at -2% rotation)

**Fig. 11:** Vierendeel mechanism

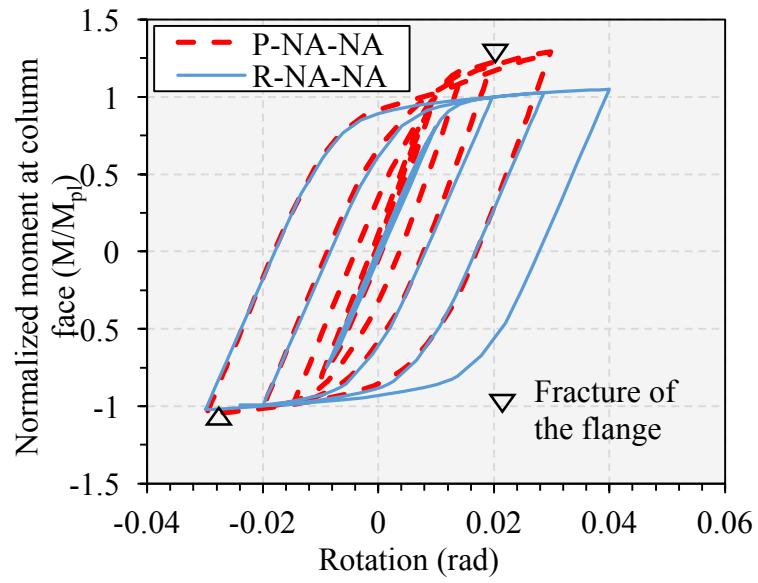


**Fig. 12:** Normalized moment-rotation curve for conventional connections (non-composite and composite)

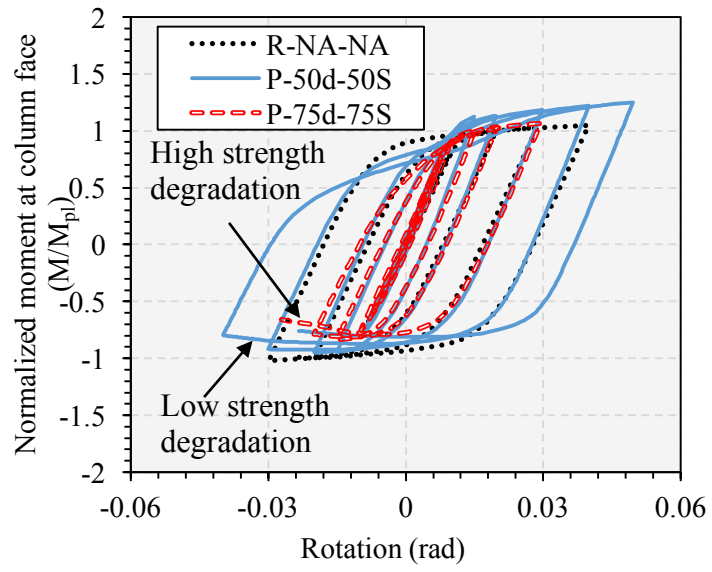


**Fig. 13:** Effect of failure mode on the ultimate rotation

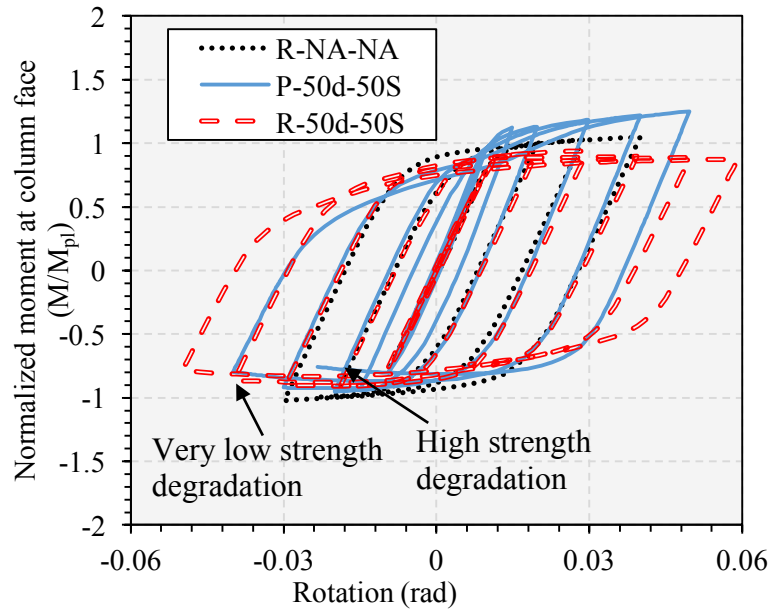
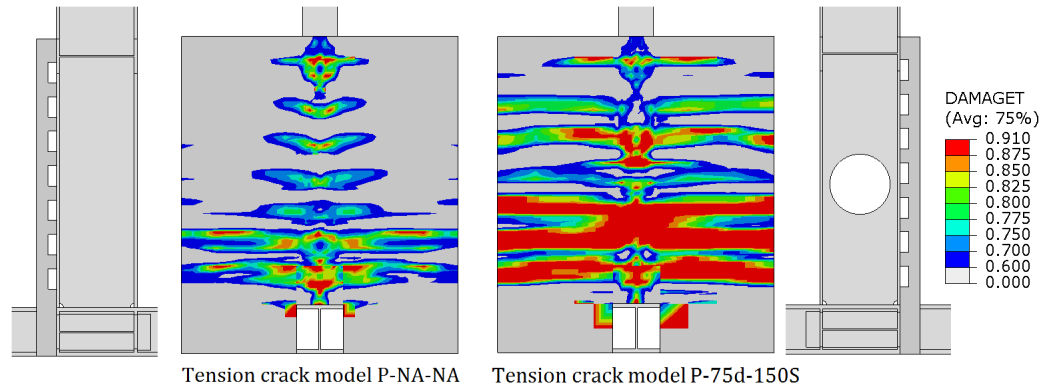


**Fig. 14:** Comparison between strength degradation of non-composite and composite RWS connections

a) Tension crack at 0.02 negative rotation



b) Concrete crushing at 0.02 positive rotation

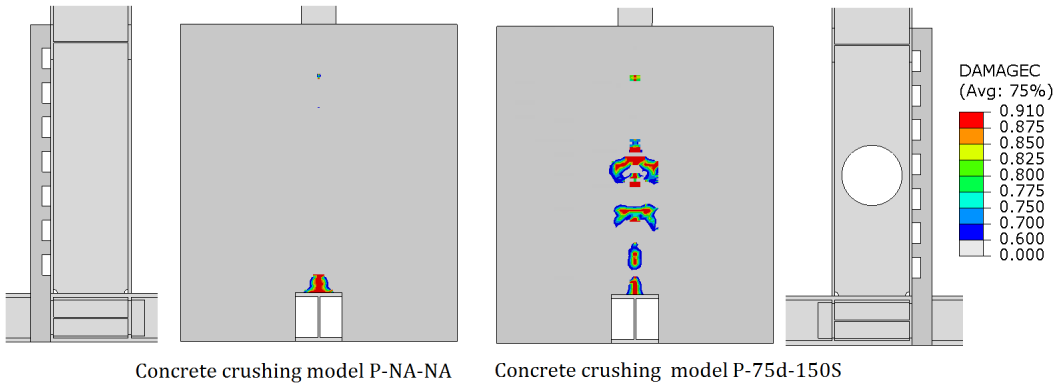
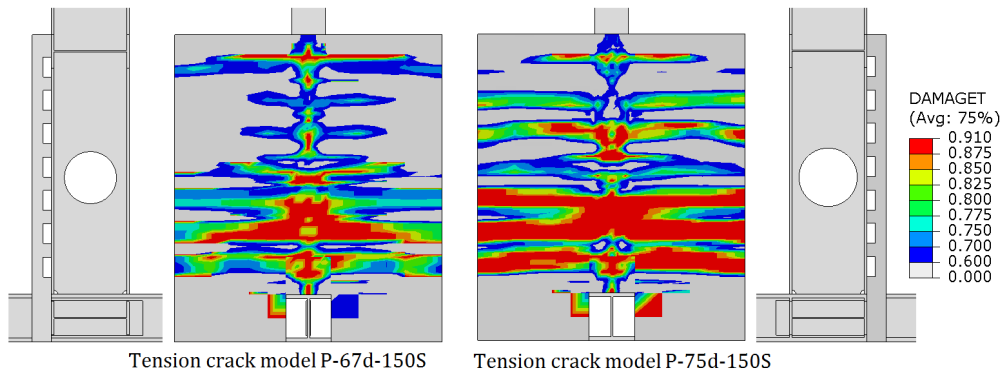


**Fig. 15:** Effect of web opening on damage in slab

a) Tension crack at 0.02 negative rotation



b) Concrete crushing at 0.02 positive rotation

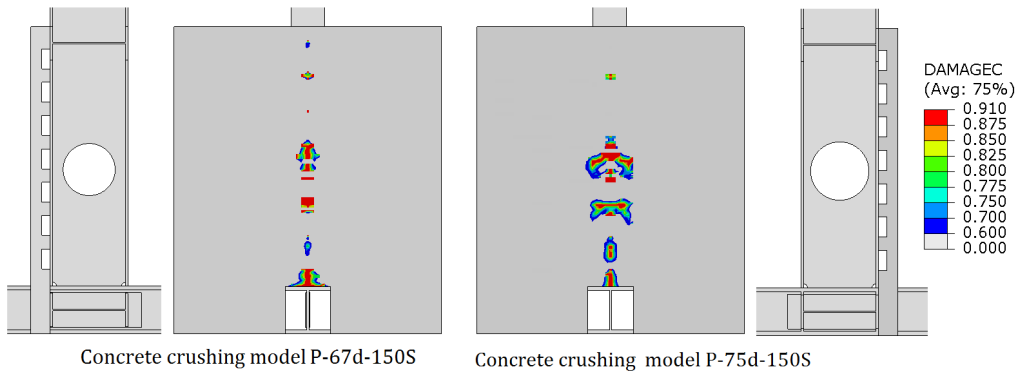


**Fig. 16:** Effect of WOA on damage in slab

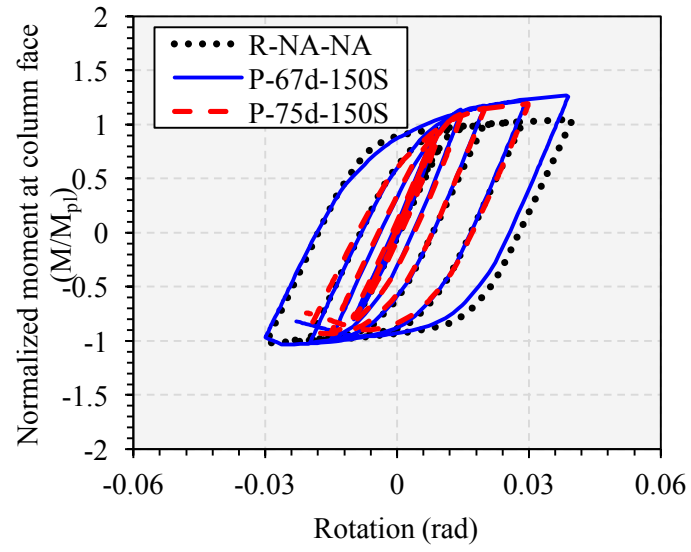


**Fig. 17:** Effect of the WOA on the capacity

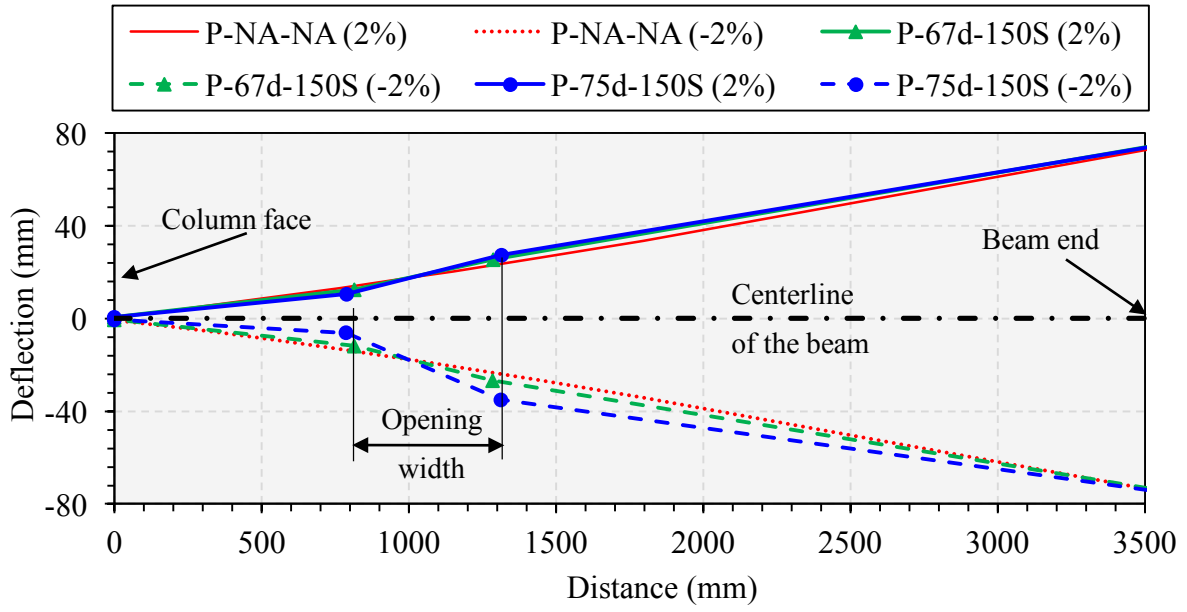


**Fig. 18:** Vertical deflection along the beam length at  $\pm 2\%$  rotation

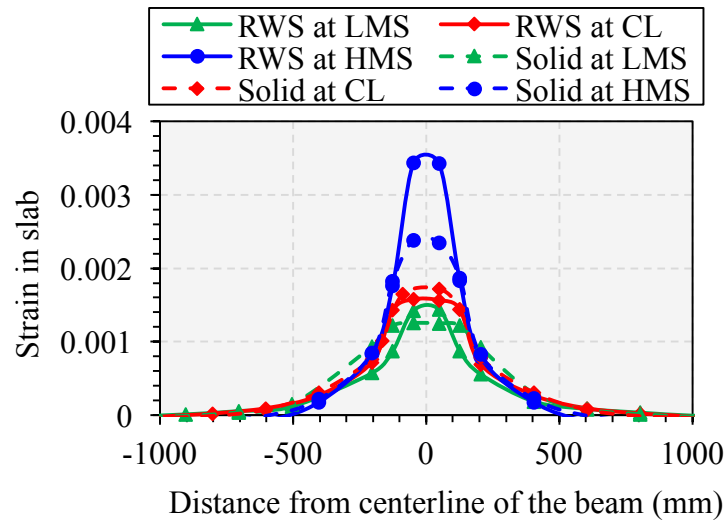


**Fig. 19:** Typical Strain in the slab for unperforated and RWS connection (at 2% story drift)

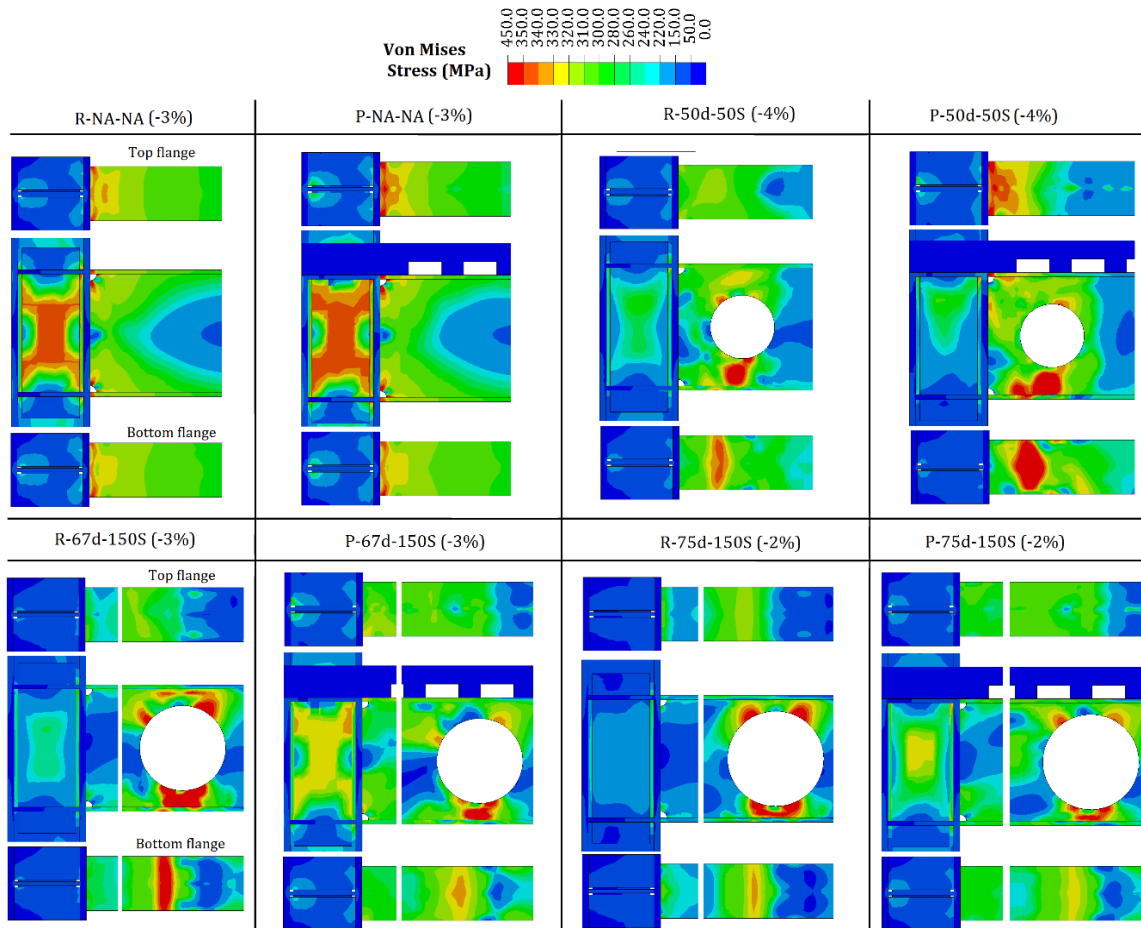


**Fig. 20:** Stress distribution

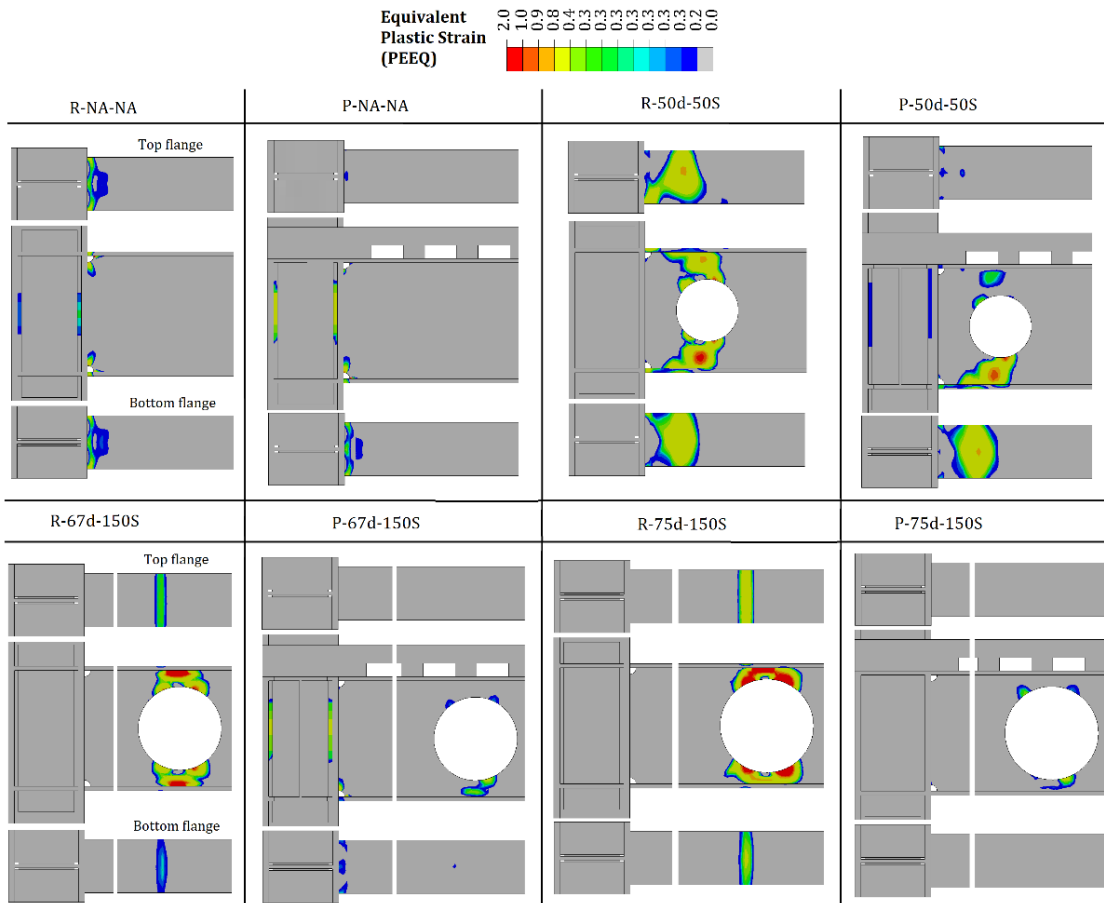


**Fig. 21:** Strain distribution